The intersection of genetic and chemical genomic screens identifies GSK-3α as a target in human acute myeloid leukemia

Versha Banerji,[1] Stacey M. Frumm,[1] Kenneth N. Ross,[2] Loretta S. Li,[1] Anna C. Schinzel,[2,3] Cynthia K. Hahn,[1] Rose M. Kakoza,[1] Kwan T. Chow,[1] Linda Ross,[1] Gabriela Alexe,[1] Nicola Tolliday,[2] Haig Inguilizian,[1] Ilene Galinsky,[3] Richard M. Stone,[3] Daniel J. DeAngelo,[3] Giovanni Roti,[1] Jon C. Aster,[4] William C. Hahn,[2,3,5] Andrew L. Kung,[1] and Kimberly Stegmaier[1,2]

[1]Department of Pediatric Oncology, Dana-Farber Cancer Institute, and Division of Hematology/Oncology, Children's Hospital Boston, Boston, Massachusetts, USA. [2]Broad Institute of Massachusetts Institute of Technology and Harvard University, Cambridge, Massachusetts, USA. [3]Department of Medical Oncology, Dana-Farber Cancer Institute, Boston, Massachusetts, USA. [4]Department of Pathology and [5]Department of Medicine, Brigham and Women's Hospital, Boston, Massachusetts, USA.

Acute myeloid leukemia (AML) is the most common form of acute leukemia in adults. Long-term survival of patients with AML has changed little over the past decade, necessitating the identification and validation of new AML targets. Integration of genomic approaches with small-molecule and genetically based high-throughput screening holds the promise of improved discovery of candidate targets for cancer therapy. Here, we identified a role for glycogen synthase kinase 3α (GSK-3α) in AML by performing 2 independent small-molecule library screens and an shRNA screen for perturbations that induced a differentiation expression signature in AML cells. GSK-3 is a serine-threonine kinase involved in diverse cellular processes, including differentiation, signal transduction, cell cycle regulation, and proliferation. We demonstrated that specific loss of GSK-3α induced differentiation in AML by multiple measurements, including induction of gene expression signatures, morphological changes, and cell surface markers consistent with myeloid maturation. GSK-3α–specific suppression also led to impaired growth and proliferation in vitro, induction of apoptosis, loss of colony formation in methylcellulose, and anti-AML activity in vivo. Although the role of GSK-3β has been well studied in cancer development, these studies support a role for GSK-3α in AML.

Introduction

Cure rates for patients with acute myeloid leukemia (AML) have changed little over the past decade. Only a minority of patients are long-term survivors, and existing high-dose chemotherapy regimens and/or stem cell transplantation have significant short- and long-term morbidity (1–3). This seemingly slow progress in improving outcomes for patients with AML is in sharp contrast to the tempo of laboratory-based discovery. New genomic approaches have dramatically altered the pace of identifying candidate molecular lesions in human disease, including AML (4, 5). The challenge now is to functionally validate emerging targets and to harness this knowledge toward therapeutic benefit.

To this end, we have extended genomic approaches to small-molecule and genetically based high-throughput screening. In particular, we have focused on the identification and validation of new AML differentiation targets. AML is characterized by both defects in proliferation and differentiation, with current therapy primarily focused on the proliferation defect (6). The success of all-*trans* retinoic acid (ATRA) differentiation therapy in the treatment of patients with the AML subtype acute promyelocytic leukemia (APL) supports the notion of differentiation therapy for AML more broadly (1, 7). Efforts to identify new differentiation agents have been hampered by lack of knowledge of a druggable target and the inherent challenges of traditional cell-based phenotypic screening. In order to address these limitations, our laboratory developed a gene expression–based high-throughput screening (GE-HTS) approach, in which gene expression signatures serve as surrogates for different biological states, in this case AML versus mature myeloid cells (8–10). Using the intersection of chemical biology and high-throughput genetic screening, we sought to identify AML differentiation targets by measuring the induction of a complex gene expression signature indicative of myeloid maturation. Glycogen synthase kinase 3α (GSK-3α) emerged as a top candidate.

GSK-3 is a multifunctional serine threonine kinase involved in diverse cellular processes, including differentiation, signal transduction, cell cycle regulation, and proliferation, with an emerging role in human malignancy (11, 12). GSK-3β has been reported as a candidate target in leukemia and other malignancies (13–18). In this manuscript, we report a role for GSK-3α in human AML.

Results

Intersection of chemical and genetic screens identifies loss of GSK-3α as a modulator of differentiation. We conducted 2 independent small-molecule library screens using a gene expression signature as a read-out for myeloid differentiation. Signature genes were measured with the previously described GE-HTS approach, using ligation-mediated amplification (LMA) and a fluorescent bead-based detection system (8–10). 3,517 compounds from the Spectrum/Prestwick Bioactives library and Harvard Stem Cells Bioactives library were screened in triplicate in the AML cell line HL-60. We independently

Authorship note: Stacey M. Frumm and Kenneth N. Ross contributed equally to this work.

Conflict of interest: The authors have declared that no conflict of interest exists.

Citation for this article: *J Clin Invest.* 2012;122(3):935–947. doi:10.1172/JCI46465.

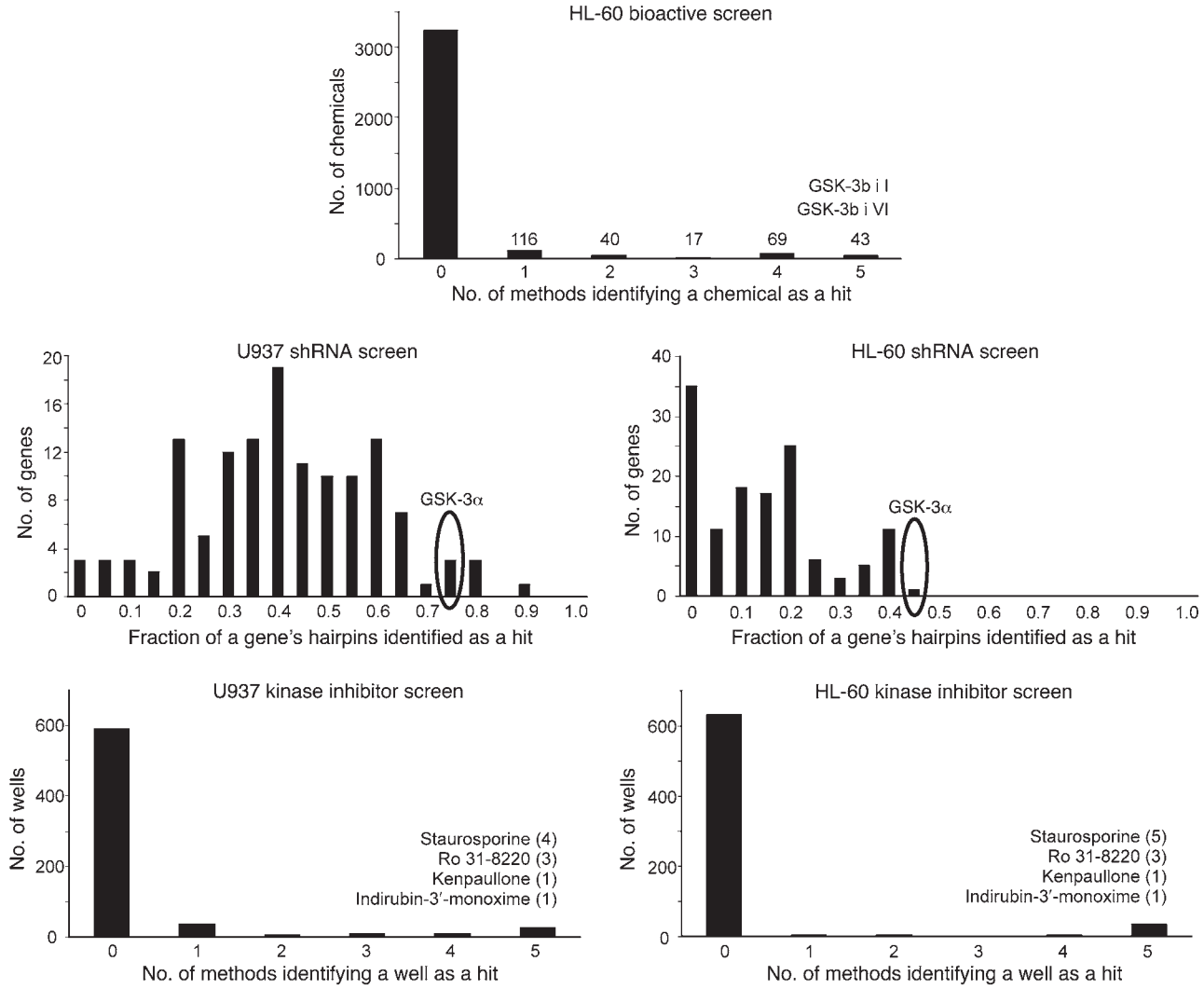

Figure 1

Three expression-based screens identify GSK-3α as a target of AML differentiation. We performed 3 independent GE-HTS differentiation screens: (a) a bioactive small-molecule library screen in HL-60 cells, (b) a kinome-focused shRNA library screen in U937 and HL-60 cells, and (c) a kinase inhibitor-focused small-molecule library screen in U937 and HL-60 cells. Perturbations were scored by consensus classification with 5 algorithms: summed score, weighted summed score, naive Bayes, K-nearest neighbor, and support vector machine. A compound or an shRNA was considered a hit if it was classified as differentiated by all 5 methods. For the bioactive screen, each compound was screened at 1 dose. 3,232 compounds did not score across any of the 5 scoring metrics. The number of compounds scoring is indicated above each histogram bar. In the shRNA screen, the fraction of hairpins that scored for each gene is depicted. For the kinase inhibitor small-molecule screen, compounds were pinned at multiple concentrations. The number of chemical wells scoring across the number of indicated scoring algorithms is depicted. Four GSK-3 inhibitors scored across all 5 methods. The number of doses that scored is indicated in parentheses. GSK-3b i I, GSK-3b Inhibitor I; GSK-3b i VI, GSK-3b Inhibitor VI.

screened a collection of 84 kinase inhibitors in 2 AML cell lines, HL-60 and U937, again measuring a complex myeloid differentiation signature. Multiple pan-GSK-3 inhibitors scored in both screens (Figure 1). Independently, a genetic screen was conducted of a kinome-focused sublibrary of the RNAi Consortium short hairpin RNA (shRNA) library, composed of 5,036 shRNAs that target 1,000 genes. This lentivirally delivered library was screened in HL-60 cells in the primary screen and then in both HL-60 and U937 cells in the secondary screen, with the myeloid differentiation signature assayed. GSK-3 also emerged as a top candidate, with shRNAs specific for GSK-3α scoring highly (Figure 1).

Chemical inhibition of GSK-3 induces differentiation in AML cell lines. Compounds identified across the chemical screens included the pan-GSK-3 inhibitors: indirubin-3′-monoxime, kenpaullone, Ro 31-8220, staurosporine, GSK-3b Inhibitor I, and GSK-3b Inhibitor VI. Neither cytosine arabinoside nor daunorubicin, 2 cytotoxics currently used in AML therapy, scored in the primary screen, suggesting that the GE-HTS differentiation assay is not merely a measurement of toxicity. We next confirmed that these small molecules induce the differentiation signature by GE-HTS in a dose-dependant manner (Supplemental Figure 1; supplemental material available online with this article; doi:10.1172/JCI46465DS1). In

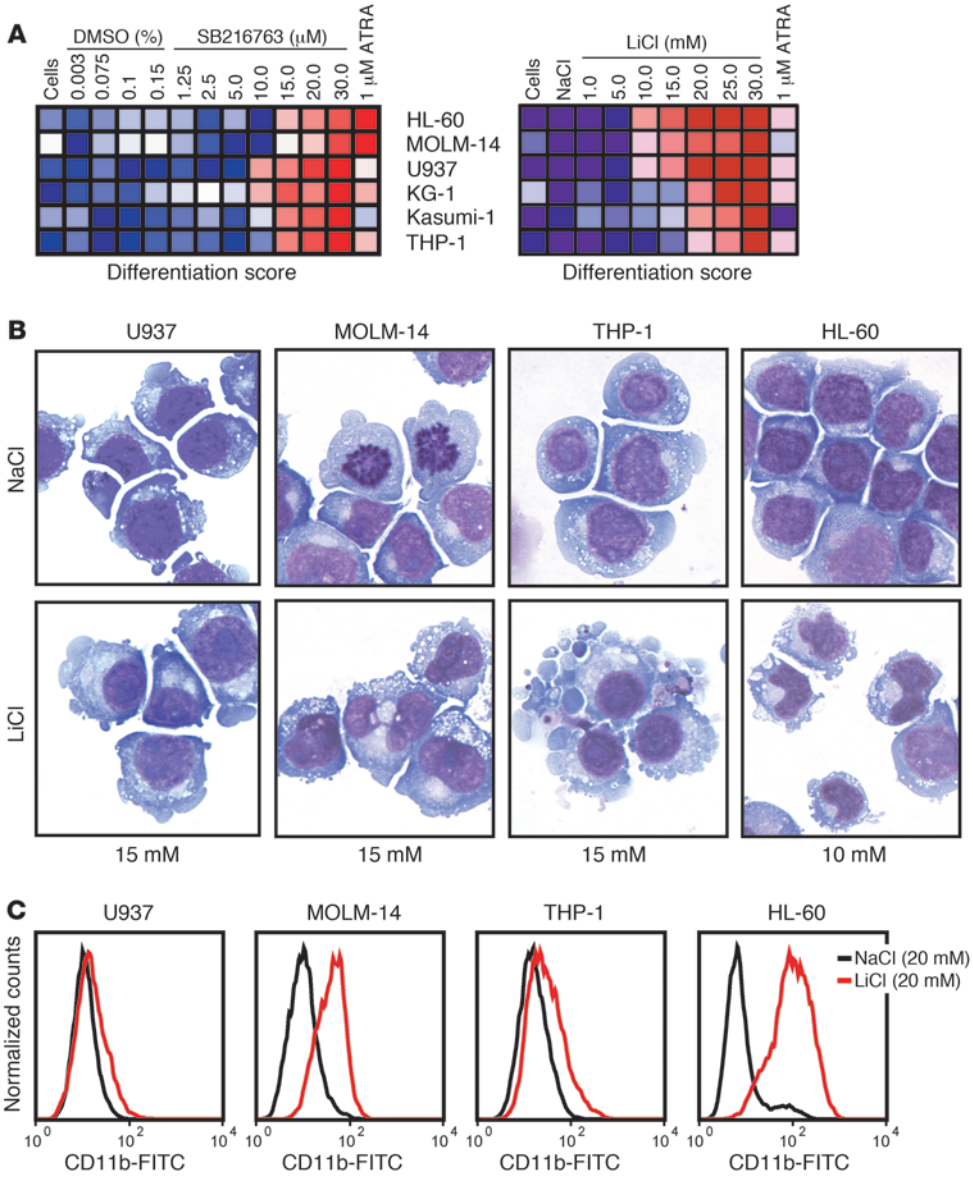

Figure 2
Pan-GSK-3 inhibition induces AML differentiation in cell lines in vitro. (**A**) AML cell lines were treated with SB216763 versus DMSO and LiCl versus NaCl for 3 days. The differentiation score (summed score), as determined using the GE-HTS assay, is depicted. 1 μM ATRA was used as the positive control. Red indicates signature induction. (**B**) May-Grunwald Giemsa staining of AML cell lines after 3 days of LiCl treatment demonstrates cellular differentiation compared with that in NaCl-treated controls. Images were acquired by light microscopy under oil with an Olympus BX41 microscope and Q-capture software (original magnification, ×1,000). (**C**) Histograms depicting an increase in CD11b staining by flow cytometry with 20 mM LiCl versus 20 mM NaCl after 5 days of treatment.

order to further validate the results of this small-molecule library screen, we tested 2 commonly used pan-GSK-3 inhibitors not in the original screen: a tool compound SB216763 (an ATP competitive inhibitor of GSK-3) and lithium chloride (LiCl) (a direct inhibitor that indirectly enhances N-terminal phosphorylation of the inhibitory phosphorylation sites). For subsequent experiments, we chose to focus on these 2 pan-GSK-3 inhibitors: SB216763, because of its frequent use in other studies, and LiCl, because of its clinical relevance. Although the compounds inactivate GSK-3 by different mechanisms, neither is isoform specific, and both the GSK-3α and GSK-3β isoforms are inhibited. We evaluated 6 AML cell lines after 3 days of treatment with SB216763 and LiCl and observed induction of the differentiation signature in a dose-dependant manner across all cell lines (Figure 2A). In addition, we evaluated morphologic changes in U937, MOLM-14, THP-1, and HL-60 cells. We observed changes consistent with macrophage-like differentiation, with a decreased nuclear-to-cytoplasmic ratio, condensation of the nucleus, and cytoplasmic ruffling (Figure 2B and Table 1). There was also evidence of myeloid maturation, as measured by an increase in expression of the surface marker CD11b (Figure 2C). We noted that these AML cell lines represent both mixed-lineage leukemia–rearranged (MLL-rearranged) and MLL wild-type disease. As in the recent report by Wang et al., we also failed to see specificity of response in a viability-based assay for MLL-rearranged human AML (Supplemental Figure 2 and ref. 13). These results indicate that pan-GSK-3 inhibition induces myeloid maturation in AML cells in vitro, independent of the presence of the MLL rearrangement.

GSK-3 inhibition differentiates primary patient blasts in vitro. Because small-molecule treatment of cell lines does not always recapitulate the effects of treatment of primary patient cells, we extended testing of pan-GSK-3 inhibitors to primary patient AML blasts. In Figure 3, we demonstrate the induction of the differentiation score by GE-HTS as well as the corresponding morphologic changes after 3 days of LiCl treatment across multiple primary samples in vitro (Figure 3 and Supplemental Table 1). There was a response to at

Table 1
Differentiation in LiCl-treated AML cell lines

Sample	Blasts (%)	Differentiating[A] (%)
THP-1 NaCl	100	0
THP-1 LiCl (15 mM)	82	18
U937 NaCl	100	0
U937 LiCl (15 mM)	54	46
HL-60 NaCl	100	0
HL-60 LiCl (10 mM)	29	71
MOLM-14 NaCl	95	5
MOLM-14 LiCl (15 mM)	20	80

Percentages shown are based on a 200 cell count. [A]Differentiating denotes cells with increased cytoplasm, cytoplasmic vacuolation, and blebbing and changes in nuclear morphology consistent with myeloid differentiation.

least 1 dose of LiCl in 7 out of 10 samples and a dose response in 4 out of 7 samples. Additionally, 3 out of 10 samples responded with a dose response to SB216763 (Supplemental Figure 3A). A 200-count differential for a subset of the patients is listed in Supplemental Figure 3B.

Loss of GSK-3α leads to differentiation of AML cells in vitro. Currently available small-molecule inhibitors of GSK-3 target both the α and β isoforms. In order to dissect whether simultaneous inhibition of both isoforms was necessary for the signature induction in human AML cells in vitro, we used an shRNA screen targeting the kinome. In both our primary and secondary shRNA screens, GSK-3α emerged as one of the top hits in 2 AML cell lines, HL-60 and U937 (Figure 1). We used a consensus classification system, with 5 scoring metrics to identify candidate shRNAs (9). In order to be considered a hit, the shRNA needed to score across all 5 scoring metrics. Two out of five shRNAs against GSK-3α scored in HL-60 cells and 4 out of 5 shRNAs against GSK-3α scored in U937 cells in the secondary screen. shRNAs against the GSK-3β isoform did not score highly in the primary screen and thus were not evaluated in the secondary screen. However, given the high degree of homology between the GSK-3α and GSK-3β isoforms, we confirmed that the shRNAs in the library had specificity for their respective isoforms and that the relative degree of knockdown was similar (Supplemental Figure 4, A and B, and Supplemental Table 2). In order to confirm the results of the screen, we cross-validated these findings in 2 additional AML cell lines, MOLM-14 and THP-1, each of which expresses an *MLL* rearrangement. Loss of GSK-3α across all 4 AML cell lines induced differentiation, as measured by changes in gene expression and alteration of cellular morphology (Figure 4, A and B). Genome-wide expression profiling was then performed, comparing the effects of shRNAs targeting GSK-3α or GSK-3β with the effects of a scrambled control shRNA (shControl). Two shRNAs for each isoform were evaluated in 4 AML cell lines (HL-60, MOLM-14, THP-1, and U937). GSK-3α suppression was enriched for gene sets associated with monocyte differentiation, which were generated from a comprehensive gene expression data set profiling cord blood samples sorted for various stages of hematopoietic differentiation (Figure 4C and ref. 19). GSK-3β suppression, in contrast, was not enriched for the same gene sets. The effects of loss of GSK-3α on differentiation were further characterized in U937 and MOLM-14 cells; GSK-3α–specific shRNAs induced expression of the myeloid maturation marker CD11b (Figure 4D).

Loss of GSK-3α decreases AML cell growth and proliferation, induces apoptosis in vitro, and attenuates colony formation in methylcellulose. When cells differentiate they often have decreased proliferation, undergo cell cycle arrest, and ultimately undergo apoptosis. Suppression of GSK-3α with 4 shRNAs inhibited proliferation, as measured by decreased BrdU incorporation, with a corresponding decrease in cell number over a time course compared with a control shRNA (Figure 5, A and B). Multiple GSK-3α–specific shRNAs also induced a G_1 cell cycle arrest and apoptosis and significantly impaired colony formation (Figure 5, C and D, and Figure 6A). Ectopic expression of a *GSK3A* cDNA immune to the effects of the shRNA rescued this phenotypic alteration on colony formation, suggesting that the effects of the shRNA were on-target for GSK-3α (Figure 6B). A decrease in colony formation with GSK-3β–targeting shRNAs was also observed (Figure 6A).

In vivo testing of GSK-3 inhibition in AML. In vitro studies provide valuable preclinical information, but they do not fully recapitulate response in the bone marrow microenvironment. One challenge in the direct application of pan-GSK-3 inhibitors, such as LiCl, to AML therapy is that these molecules induce stabilization of β-catenin (Supplemental Figure 4, C and D), which has been reported to promote AML self-renewal (20). Indeed, a recent study by Yeung et al. demonstrated the importance of concurrent knockdown of β-catenin with pan-GSK-3 inhibitor treatment in a mouse model of AML in order to effectively target AML-initiating cells (21). We observed that cells grown short-term in 384-well format, as in the GE-HTS screens, were not dependent on β-catenin, whereas cells grown in a more physiologically relevant ex vivo assay (i.e., methylcellulose) were dependent (Supplemental Figure 5). Because isoform-specific loss of GSK-3 does not promote stabilization of β-catenin, an alternative strategy would be isoform-selective inhibition (22).

We first confirmed that loss of GSK-3α did not stabilize β-catenin in AML cells in vitro (Supplemental Figure 4A). In addition, loss of GSK-3α did not activate *TCF*, a downstream effector of nuclear β-catenin, nor did it enrich for gene sets correlated with *WNT* or *CTNNB1* in genome-wide expression analysis by Gene Set Enrichment Analysis (GSEA) (Supplemental Figure 6).

We next extended testing of GSK-3 isoform-specific inhibition to a human AML orthotopic xenograft model in which U937 cells were labeled with luciferase (U937-LucNeo) and propagated in NOD-SCID IL2Rγ^{null} (NSG) xenografts. In our first study, loss of GSK-3α (shGSK3A_5) impaired progression of this U937 orthotopic xenograft, as measured in vivo by both bioluminescence and spleen weight (Figure 7, A and B). Using bioluminescence as a surrogate marker for disease burden, we next evaluated the effects of 2 additional shRNAs (shGSK3A_8 and shGSK3A_9) targeting the GSK-3α isoform. Both demonstrated statistically significant anti-AML activity (Figure 7C). In an independent experiment looking at the end point of survival, animals inoculated with U937-LucNeo cells expressing a fourth GSK-3α–directed shRNA (shGSK3A_6) had a survival advantage (Figure 7D). Thus, inhibition of GSK-3α impaired engraftment and impacted survival in vivo. In these studies, 1 out of 4 GSK-3β–directed shRNAs (shGSK3B_2) tested demonstrated statistically significant impairment of AML in vivo (Figure 7D and Supplemental Figure 7).

Discussion

AML remains the most common form of acute leukemia in adults and the second most common form in children. Although advances have been made in predicting outcome based upon molecu-

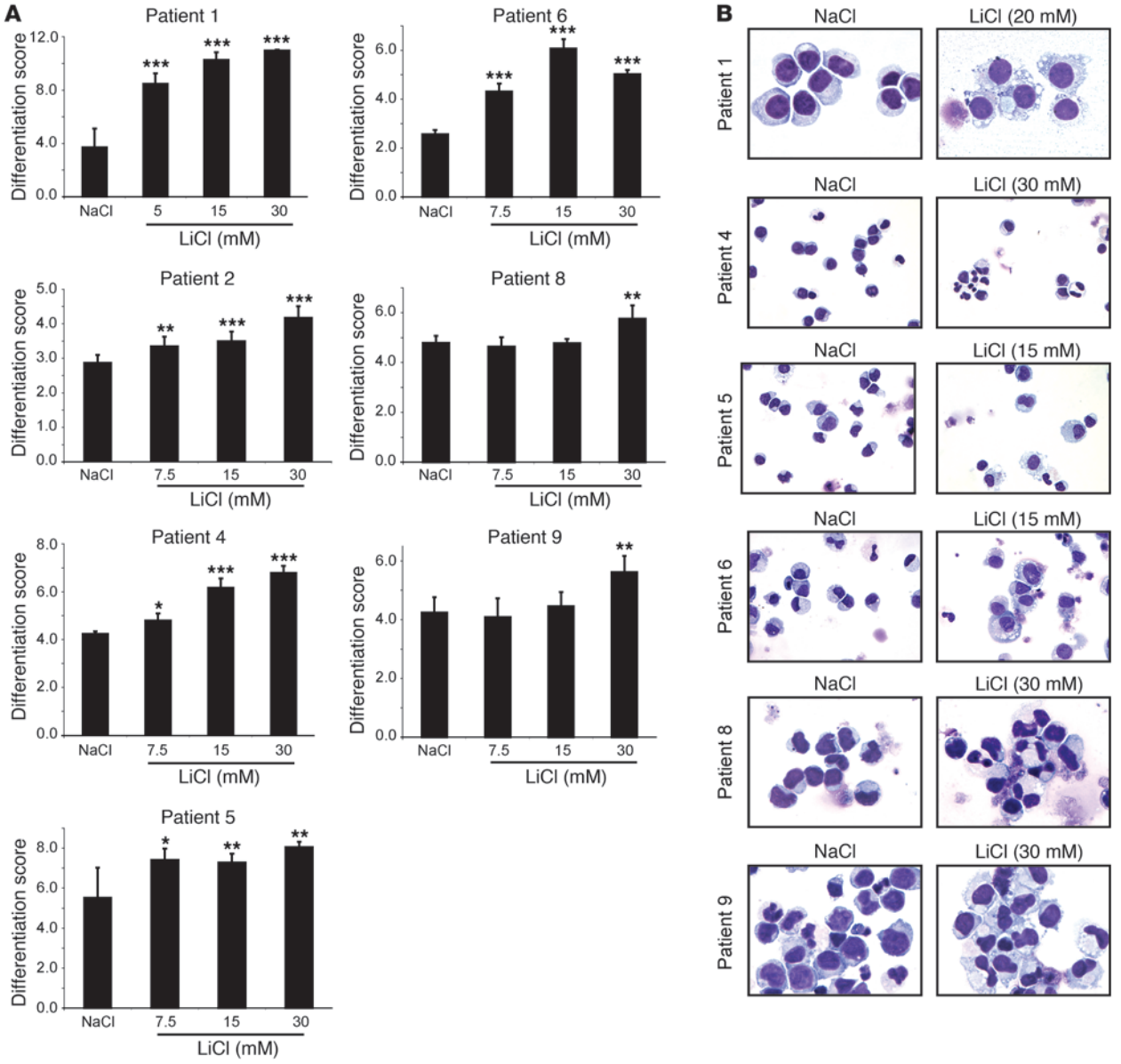

Figure 3

Pan-GSK-3 inhibition induces AML differentiation in primary patient blasts in vitro. (**A**) Histograms depicting the differentiation score (summed score) for 7 primary patient samples treated in vitro for 3 days with LiCl. Error bars represent the mean ± SD of 5 replicates. $^{*}P < 0.05$, $^{**}P < 0.01$, $^{***}P < 0.001$ by 1-way ANOVA using Tukey's multiple comparison test. (**B**) May-Grunwald Giemsa staining of primary patient blasts at day 3 after treatment with LiCl demonstrates monocyte/macrophage-like cellular differentiation compared with that in the NaCl-treated controls. Images were acquired by light microscopy under oil with an Olympus BX41 microscope and Q-capture software (original magnification, ×1,000). No cytospins were available for patient 2.

lar features, there has been little progress in the last decade in altering cure rates. One exception is the successful treatment of patients with APL, defined by the PML-RARα rearrangement, with ATRA differentiation therapy. To this end, we sought to identify alternative candidate targets for AML differentiation. We leveraged new genomic approaches for cancer discovery with the integration of signature-based small-molecule library screening and high-throughput shRNA screening. Multiple pan-GSK-3 inhibitors scored in 2 chemical screens and were confirmed to both induce differentiation and to alter cell viability in AML. We next turned to the shRNA screen to further detail the role of GSK-3. In this screen, shRNAs specifically directed against GSK-3α scored highly.

GSK-3 is a constitutively active serine threonine kinase that inhibits the Wnt and hedgehog pathways while activating NF-κB. GSK-3 has been reported to play a role in normal cellular homeostasis, including hematopoiesis (23, 24), as well as in a diversity of human diseases, such as Alzheimer disease (25), non-insulin-dependent diabetes mellitus (26), and bipolar disorder (27). More recently, and somewhat surprisingly, GSK-3 has emerged as a

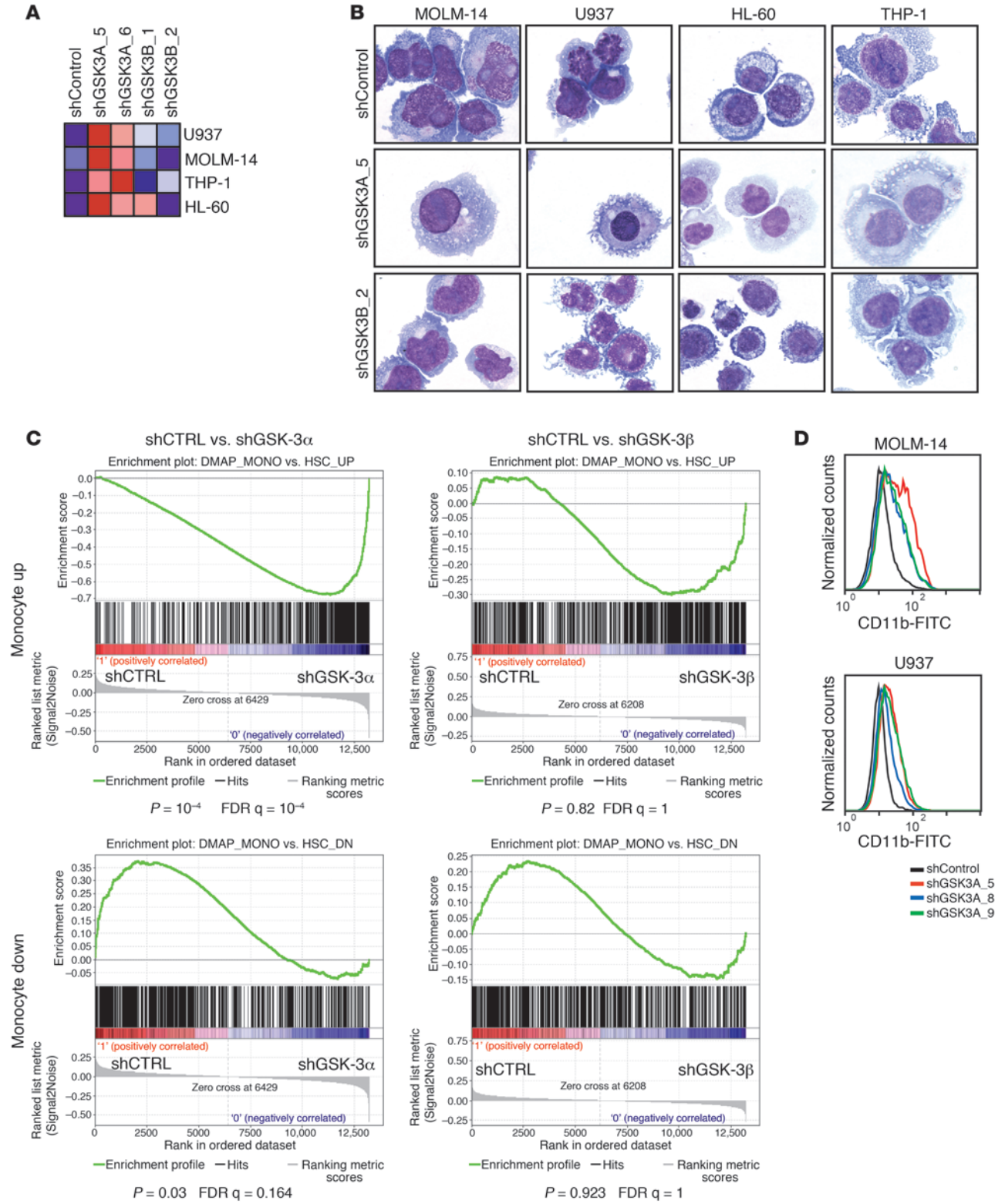
A
shControl
shGSK3A_5
shGSK3A_6
shGSK3B_1
shGSK3B_2
U937
MOLM-14
THP-1
HL-60
B
MOLM-14
U937
HL-60
THP-1
shControl
shGSK3A_5
shGSK3B_2
C
shCTRL vs. shGSK-3α
shCTRL vs. shGSK-3β
Monocyte up
Monocyte down
Enrichment plot: DMAP_MONO vs. HSC_UP
Enrichment plot: DMAP_MONO vs. HSC_DN
Enrichment score
Ranked list metric (Signal2Noise)
'1' (positively correlated)
'0' (negatively correlated)
shCTRL
shGSK-3α
shGSK-3β
Zero cross at 6429
Zero cross at 6208
Rank in ordered dataset
Enrichment profile
Hits
Ranking metric scores
P = 10⁻⁴ FDR q = 10⁻⁴
P = 0.82 FDR q = 1
P = 0.03 FDR q = 0.164
P = 0.923 FDR q = 1
D
MOLM-14
U937
Normalized counts
CD11b-FITC
shControl
shGSK3A_5
shGSK3A_8
shGSK3A_9

Figure 4
Loss of GSK-3α in AML induces differentiation in vitro. (**A**) Isoform-specific GSK-3–directed shRNAs or a control shRNA were introduced into 4 AML cell lines, and the differentiation score (summed score) was determined using the GE-HTS assay. Red indicates induction of the differentiation score. (**B**) Morphology was evaluated 7 days after infection with May-Grunwald Giemsa staining of cytospin preparations. Images were acquired by light microscopy under oil with an Olympus BX41 microscope and Q-capture software (original magnification, ×1,000). (**C**) Four AML cell lines were profiled on Affymetrix expression arrays with shRNAs directed against GSK-3α or GSK-3β in comparison to a scrambled control shRNA (shCTRL), and GSEA was performed. Enrichment plots are shown for GSK-3α and GSK-3β knockdown in gene sets associated with monocyte maturation. FDR, false discovery rate; Monocyte up, upregulated in monocytes; Monocyte down, downregulated in monocytes. (**D**) Loss of GSK-3α leads to an increase in CD11b expression by flow cytometry 6 days after infection.

target in hematological malignancies. For example, GSK-3β mis-splicing, leading to an increase in β-catenin and enhanced serial replating, was reported in the granulocyte-macrophage progenitors in blast crisis chronic myelogenous leukemia (14). Chemical inhibition of GSK-3 was also reported to induce apoptosis in chronic lymphocytic leukemia and in multiple myeloma (15, 28, 29). Moreover, GSK-3 was initially reported as a target in MLL-rearranged acute leukemia and then more broadly in hematopoietic cells transformed by HOX genes by promoting the conditional association of CREB and its coactivators CBP and TORC with MEIS1 (13, 17). Interestingly, in our genome-wide expression studies, GSK-3α–specific loss was anticorrelated with gene sets generated by the coexpression of *HOXA9* and *MEIS1* (Supplemental Figure 8). Whether GSK-3α specifically promotes CREB association warrants further study. Our genome-wide expression studies also point to the downregulation of a MYC program as another potential mechanism linking the loss of GSK-3α with induction of AML differentiation. Multiple *MYC* gene expression signatures are downregulated with loss of GSK-3α by GSEA (Supplemental Figure 9). Several studies implicate downregulation of MYC as a mechanism to promote AML differentiation, including a recent study by Zuber et al. reporting that the loss of MYC expression by small-molecule inhibition of the bromodomain-containing 4 protein (BRD4) leads to AML differentiation (30).

While these results point to GSK-3 as a target in leukemia, there are some concerns about targeting GSK-3 in AML with available pan-GSK-3 small-molecule inhibitors. In its active state, GSK-3 inhibits the Wnt pathway by phosphorylating β-catenin, marking it for proteasomal degradation. When GSK-3 is pan-inhibited, β-catenin is stabilized, enters the nucleus, and initiates its transcriptional programs (11, 22, 31, 32). Recently, Wang et al. demonstrated that reactivation of β-catenin signaling is required for the transformation of progenitor cells by certain oncogenes, including *HOXA9*, *MEIS1*, and *MLL* (20). Thus, stabilization of β-catenin with pan-GSK-3 inhibition may promote self-renewal in some AML progenitor cells. Interestingly, the pan-GSK-3 inhibitor lithium was used in the 1970–1980s in clinical trials in an attempt to decrease the time of neutropenia, based on the observation that lithium increased neutrophil counts in patients being treated for psychiatric disease (33–36). In a clinical trial, patients with AML treated with cytosine arabinoside and daunorubicin were randomized to receive lithium versus a placebo. The incidence of complete remission was actually significantly lower in patients receiving lithium (75% versus 49%; $P = 0.012$) (37). Because the doses of lithium needed to achieve maximal effect in vitro are supratherapeutic, it is possible that more potent agents would have greater activity in vivo. The potential leukemogenic effect of increasing β-catenin, however, is still a concern, even with more potent pan-GSK-3 inhibitors. In a recent report, Yeung et al. demonstrate the dependency of the MLL leukemic stem cell (LSC) compartment on β-catenin (21). They also demonstrate that the MLL LSCs are resistant to the effects of GSK-3 pan-inhibition, supporting the inadequacy of lithium as a single-agent therapy in some molecular subtypes of AML. The LSCs become sensitized to lithium in the presence of β-catenin knockdown, suggesting that pan-GSK-3 inhibition in combination with inhibition of Wnt signaling is a potential therapeutic strategy in AML (21).

An alternative, more parsimonious approach to translating our findings to the clinic might be to develop a GSK-3 isoform-specific inhibitor. Although 90% homologous in their kinase domains, the α and β isoforms of GSK-3 are not functionally redundant (11, 12, 32). For example, GSK-3α knockout mice show signs of metabolic and neuronal developmental abnormalities (38, 39), while the GSK-3β knockout is lethal late in gestation due to hepatic apoptosis, a phenotype similar to that seen in the NF-κB knockout (40, 41). However, both isoforms of GSK-3 need to be inhibited for β-catenin stabilization. Doble et al. have demonstrated through the generation of an allelic series of mouse embryonic stem cell (ESC) lines with 0 to 4 functional GSK-3 alleles that specific loss of the GSK-3α or GSK-3β alleles did not lead to an increase in β-catenin. It was only when 3 out of the 4 GSK-3 alleles were lost that a rise in β-catenin levels was observed. GSK-3α/β double-knockout ESCs displayed hyperactivated Wnt/β-catenin signaling, and their ability to differentiate was impaired (22). Moreover, as demonstrated in this report, genetic loss of either the α or β isoform in human AML does not lead to β-catenin stabilization, whereas pan-inhibition does (Supplemental Figures 4 and 6).

Although much of the literature has focused on the GSK-3β isoform, we focused on GSK-3α because it scored highly in our shRNA AML differentiation screen. Inhibition of GSK-3α with multiple shRNAs induced differentiation, as measured by induction of the GE-HTS differentiation signature, expression of myeloid surface markers, genome-wide expression changes consistent with differentiation, and induction of morphological characteristics of monocyte/macrophage-like maturation in vitro. There was also impaired cell growth and proliferation, induction of cell cycle arrest and apoptosis, and loss of colony formation in methylcellulose. Moreover, 4 GSK-3α–specific shRNAs led to a decrease in disease burden and/or prolonged survival in an in vivo model. While we hypothesize that the AML cells undergo differentiation and then ultimately arrest, as is described in APL with ATRA therapy (42), another possibility is that there is a heterogeneous response to GSK-3α inhibition, with one population undergoing differentiation and another undergoing apoptosis. Interestingly, recent studies reported a surprising role for GSK-3α inhibition in cardiomyocyte differentiation (43) and a role for GSK-3α expression in protection against apoptosis with ischemic injury to the heart (44).

In treating patients with cancer, we are in transition from an era dominated by the use of cytotoxic chemotherapy to an era with the hope of "targeted" therapy. Our results support the further refinement of potential drug targets to the granular level of isoform

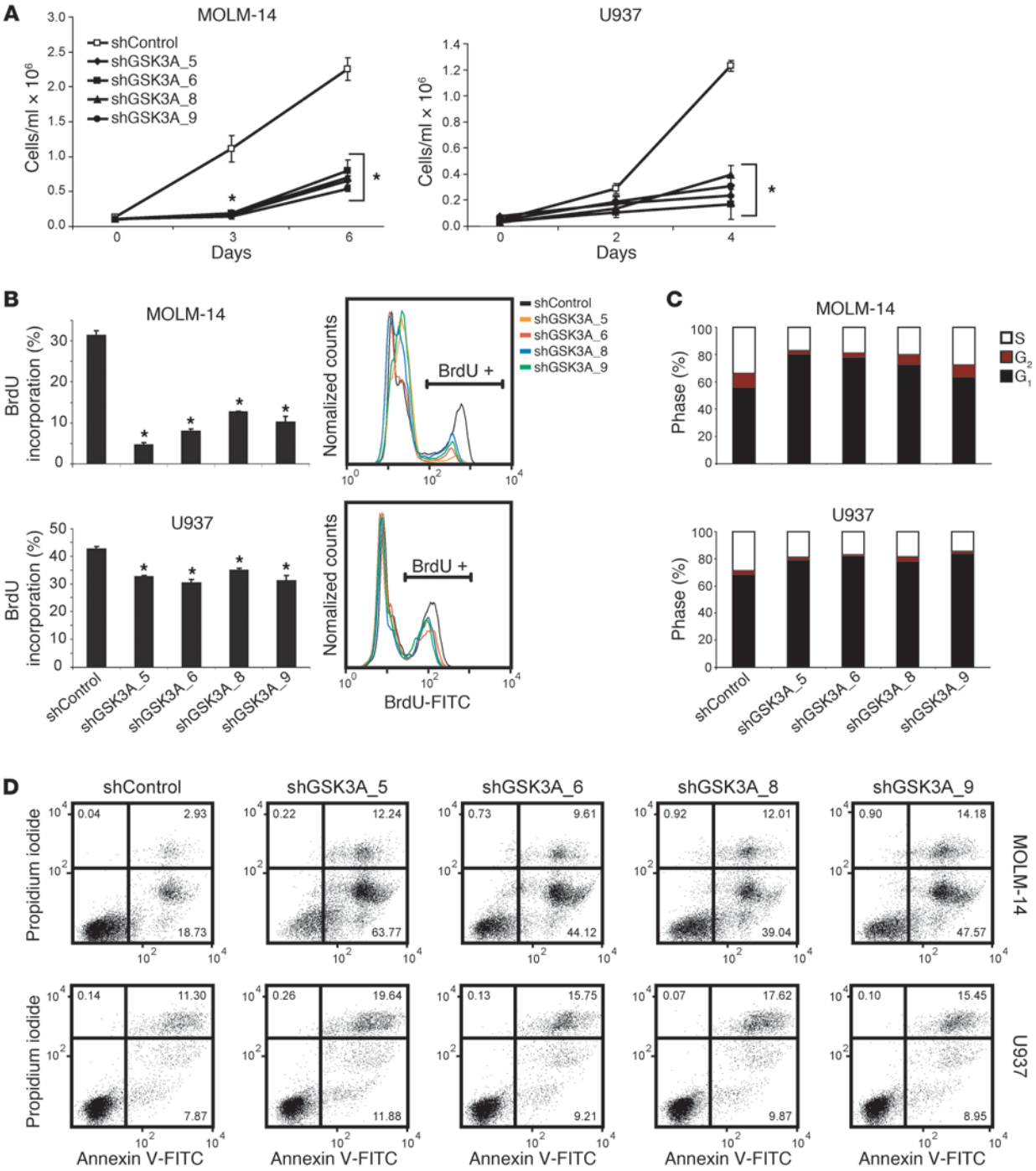

Figure 5

Phenotypic alterations associated with GSK-3α loss in MOLM-14 and U937 cells. (**A**) Cell number, as measured by trypan blue exclusion. Shown are the mean ± SD of 3 replicates. *$P < 0.001$ by 2-way repeated-measures ANOVA, with a Bonferroni post-hoc test comparing each shRNA to the shControl. The effects of GSK-3α suppression on (**B**) BrdU incorporation, (**C**) cell cycle, and (**D**) apoptosis are depicted. In **B**, the mean ± SD of 3 biological replicates is shown on the left, and a representative experiment is shown on the right. *$P < 0.001$ by 1-way ANOVA with Tukey's multiple comparison test. In **C** and **D**, representative experiments of 2 biological replicates are shown. In **D**, numbers represent percentages of cells in each quadrant.

specificity. Indeed, with the recognition of the nonoverlapping roles of phosphoinositide 3-kinase (PI3K) isoforms in malignancy, the development of PI3K isoform-specific inhibitors is already well underway (45). To our knowledge, no GSK-3α–specific small-molecule inhibitors have been described and a reported GSK-3β–selective molecule is not yet commercially available (46). Given the high degree of homology of the kinase domains of the α and β isoforms, one potential strategy would be to develop an allosteric

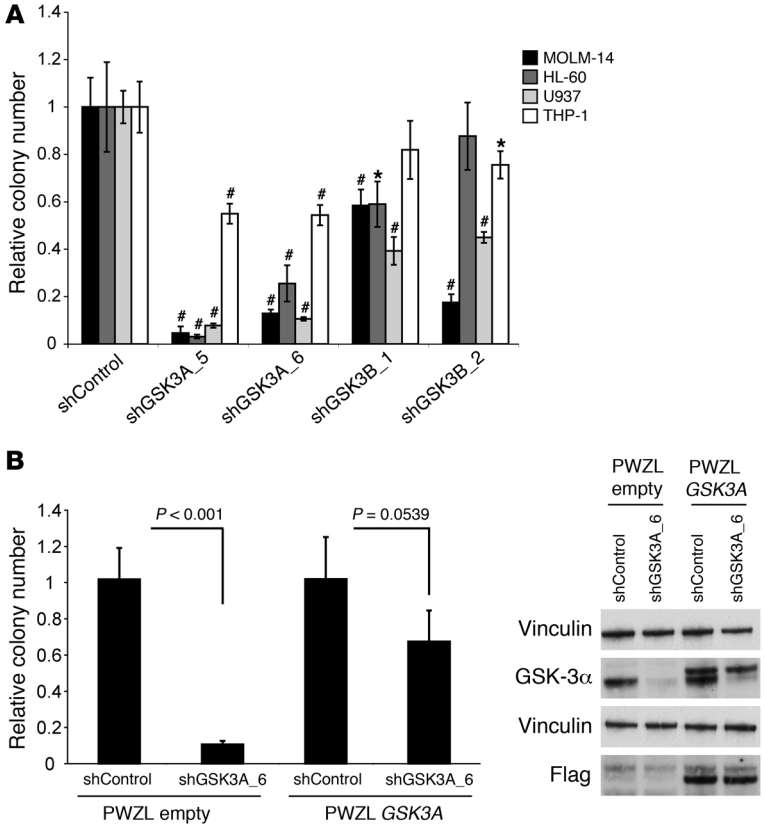

Figure 6
Isoform-specific loss of GSK-3 impairs colony formation in methylcellulose. (**A**) AML cell lines were infected with isoform-specific GSK-3–directed shRNAs or a control shRNA and plated in methylcellulose. The graph illustrates the relative number of colonies as a ratio to that in shControl. Data represent mean ± SD of 2 biological replicates. $^{*}P < 0.01$, $^{\#}P < 0.001$ by 1-way ANOVA using Tukey's multiple comparison test. (**B**) In MOLM-14 cells, overexpression of a GSK-3α cDNA immune to the effects of the 3′ UTR–directed hairpin shGSK3A_6 rescues the colony formation phenotype caused by GSK-3α knockdown. Data represent mean ± SD of 2 biological replicates. Significance was calculated by Student's *t* test. The immunoblot demonstrates GSK-3α overexpression and loss of the endogenous protein with shGSK3A_6.

small-molecule inhibitor of GSK-3α or GSK-3β. While our studies demonstrate a more potent effect with shRNA directed against GSK-3α compared with that directed against GSK-3β, there are several possible explanations for this observation. Though our immunoblot quantification suggests near equivalent relative protein knockdown, such measurements are notoriously imprecise. Thus, subtle differences in knockdown could contribute to a difference in the observed phenotype, or the full phenotypic effect may require complete loss of GSK-3β. Moreover, the slower kinetics of loss of GSK-3 with shRNA may alter the phenotype observed compared with that of a small-molecule inhibitor, and the loss of the protein may induce a phenotype different from loss of its enzymatic activity. Indeed, it will be important to test both GSK-3α– and GSK-3β–selective small-molecule inhibitors as these molecules are characterized.

In summary, these studies suggest a role for GSK-3α in AML differentiation and support a potential role for GSK-3α–directed targeted therapy. Moreover, they illustrate the strength of integrating multiple orthogonal screens toward cancer target identification.

Methods

Cell culture

Primary patient AML blasts were collected from peripheral blood or bone marrow aspirate, after obtaining informed consent of patients under Dana-Farber Cancer Institute Internal Review Board–approved protocols. Mononuclear cells were isolated using Ficoll-Paque Plus (Amersham Biosciences), and red blood cells were lysed (eBioscience). HL-60, U937, Kasumi-1, and KG-1 cells were purchased from ATCC. Scott Armstrong provided THP-1, MOLM-14, and MV4-11 cell lines. SKNO-1 cells were provided by Jonathan Licht. All cell lines and primary patient cells were maintained in RPMI 1640 (Cellgro) supplemented with 1% penicillin-streptomycin (PS) (Cellgro) and 10% FBS (Sigma-Aldrich) at 37°C with 5% CO_2.

Compounds

Compounds were obtained from the following sources: indirubin-3′-monoxime, kenpaullone, and Ro 31-8220 (all from ENZO Life Sciences); GSK-3b Inhibitor I and GSK-3b Inhibitor VI (both from Calbiochem); vorinostat (Broad Chemistry Program); SB216763, DMSO, and LiCl (all from Sigma-Aldrich); and sodium chloride (SAFC Biosciences). All compounds were diluted in DMSO with the exception of LiCl and sodium chloride, which were diluted in water and filter sterilized.

Morphological evaluation

On day 7 after infection and day 3 after chemical treatment, cytospin preparations were performed. Changes in cellular morphology were evaluated by May-Grunwald Giemsa staining (Sigma-Aldrich). Images were acquired by light microscopy under oil at ×1,000 magnification with an Olympus BX41 microscope and Q-capture software.

Viability assays

Cell lines were incubated with compounds in 384-well format. Viability was evaluated with the CellTiter-Glo Luminescent Cell Viability Assay (Promega) after 3 days of incubation. Luminescence was measured using a FLUOstar Omega from BMG Labtech. Cell number was determined using trypan blue exclusion over a time course.

Flow cytometry

The surface marker CD11b was measured at day 5 after chemical treatment and day 6 after infection (Beckman Coulter no. IM0530U). Cell cycle was

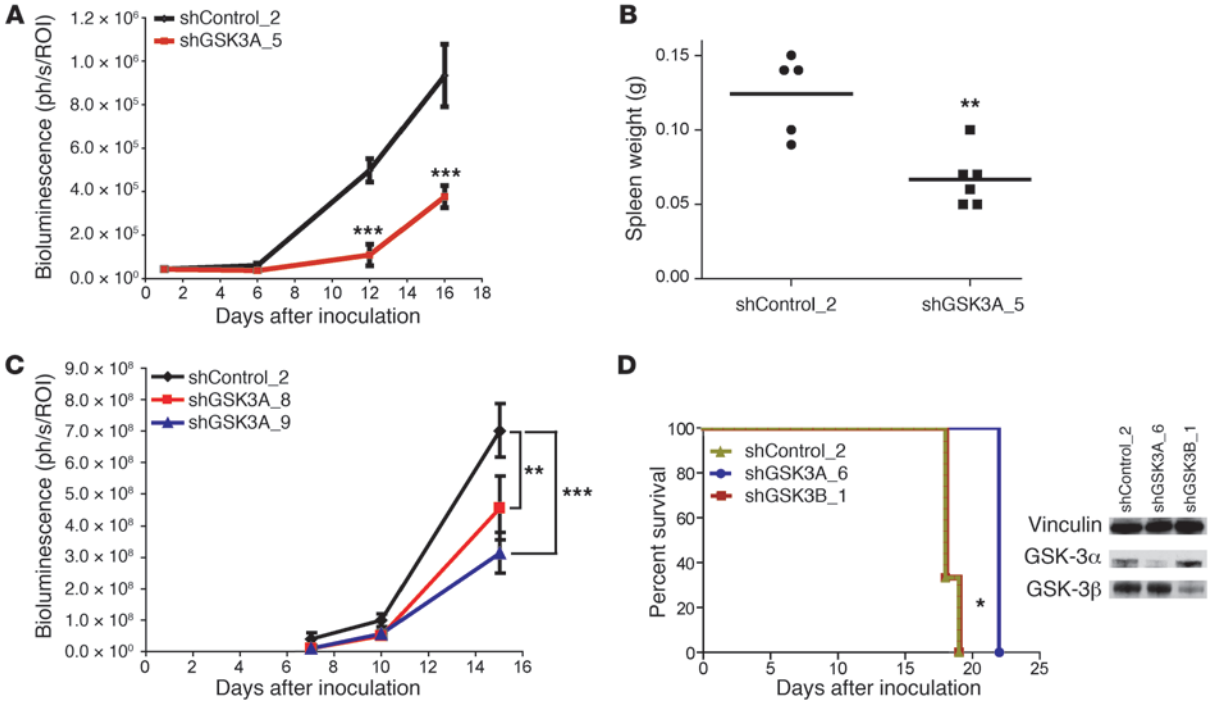

Figure 7

GSK-3α loss has anti-AML activity in vivo. (**A**) U937-LucNeo cells infected with pLKO.1 vectors against GSK-3α (shGSK3A_5) and lacZ (shControl_2) were injected on day 0. Bioluminescence was quantified as a measure of disease burden. Data are represented as mean ± SEM of 6 mice per cohort. ***$P < 0.001$ by 2-way repeated-measures ANOVA, with a Bonferroni post-hoc test comparing shGSK3A_5 with shControl_2. (**B**) Spleen weights were measured on day 20 after injection. There were 5 mice in the shControl_2 cohort and 6 mice in the shGSK3A_5 cohort. Each symbol represents an individual mouse, and horizontal bars represent mean values. **$P < 0.01$ by Student's *t* test. (**C**) U937-LucNeo cells infected with pLKO.1 vectors against GSK-3α (shGSK3A_8 and shGSK3A_9) and lacZ (shControl_2) were injected on day 0. Bioluminescence was quantified as a measure of disease burden. Data are represented as mean ± SEM of 6 mice per cohort. **$P < 0.01$, ***$P < 0.001$ by 2-way repeated-measures ANOVA, with a Bonferroni post-hoc test comparing each shRNA to shControl_2. (**D**) Survival is shown for mice engrafted with U937-LucNeo cells infected with pLKO.1 vectors against GSK-3α (shGSK3A_6), GSK-3β (shGSK3B_1), and lacZ (shControl_2). Mice were engrafted on day 0. There were 6 mice in each cohort, with statistical significance calculated by log-rank test. *$P < 0.05$, shGSK3A_6 survival curve relative to shControl_2 survival curve.

measured using PI staining for DNA content at day 6 after infection in U937 cells and day 4 after infection in MOLM-14 cells. Proliferation was measured using the FITC BrdU Flow Kit as per the manufacturer's protocol (BD Pharmingen) after a 1-hour BrdU pulse on day 5 after infection. Apoptosis was measured using the FITC Annexin V Apoptosis Detection Kit as per the manufacturer's protocol (BD Pharmingen) 4 days after infection in U937 cells and 6 days after infection in MOLM-14 cells.

Viral vectors and infection

Sequences targeted by each GSK-3α/β shRNA are listed in Supplemental Table 3. For large scale infections, 2×10^6 HEK293T cells were plated in 10-cm plates and transfected 24 hours later with 3 μg DNA from pLKO.1 lentiviral vector and packaging plasmids (pCMV8.9 and pCMV-VSVG) according to the FuGENE 6 (Roche) protocol. Medium was changed 24 hours after transfection, and viral supernatant was harvested every 8 hours for the subsequent 48 hours and filtered using 0.45-μm filters. AML cell lines were infected for 2 hours at 37°C with 2 ml lentiviral supernatant and 8 μg/ml polybrene (Sigma-Aldrich) and then diluted to 10 ml with medium. Cells were selected 48 hours later with 1 μg/ml puromycin (Sigma-Aldrich). Rescue experiments were conducted using a pWZL empty vector and a pWZL *GSK3A* cDNA. 2×10^6 HEK293T cells were plated in 10-cm plates and transfected 24 hours later with 10 μg DNA from retroviral backbone vector and packaging plasmids (p-N8-ε-Env and p-N8-ε-VSVG) according to the FuGENE 6 (Roche) protocol. Viral supernatant was harvested as described above. MOLM-14 cells were spin infected for 1 hour on 2 consecutive days and selected 48 hours after the second infection using 1.5 mg/ml neomycin (Invitrogen). Once stable cell lines were established, cells were infected with the lentivirally delivered shControl and shGSK3A_6 shRNAs. At 48 hours after infection, the cells were selected with 1 μg/ml puromycin. The β-catenin reporter 7xTCF-luc-puro was stably infected into MOLM-14 cells as described above.

Immunoblotting

Cells were lysed in Cell Signaling Lysis Buffer (Cell Signaling Technology), containing Complete, EDTA-free Protease Inhibitor Cocktail tablets (Roche Diagnostics), and PhosSTOP Phosphatase Inhibitor (Roche Diagnostics), resolved by gel electrophoresis using Novex 4%–12% Bis-Tris Gel (Invitrogen), transferred to nitrocellulose membranes (Bio-Rad), and blocked for 1 hour in 5% BSA (Sigma-Aldrich). Blots were incubated with primary antibodies to p-GSK-3α (S21) (Cell Signaling Technology no. 9316S), p-GSK-3β (S9) (Cell Signaling Technology no. 9336S), p-GSK-3α/β (Y279/216) (Thermo Scientific catalog no. OPA1-03083), total GSK-3α (Cell Signaling Technology no. 9338), total GSK-3β (Cell Signaling Technology no. 9315), total GSK-3α/β (Abcam ab82542), anti-Flag (Sigma-Aldrich catalog no. F1804), β-catenin (Millipore catalog no. 06-734), or Vinculin (Abcam ab18058), followed by secondary antibodies anti-rabbit HRP (Amersham NA9340V) or anti-mouse

HRP (Amersham NA9310V). Bound antibody was detected using Western Lightning Chemiluminescence Reagent (Perkin Elmer). Quantification of the Western blots was performed using ImageJ software (http://rsbweb.nih.gov/ij/). Blank readings were obtained and subtracted from all measurements to correct for background. Each protein band for GSK-3 was quantified with respect to the loading control and then normalized to the shControl (Supplemental Table 2).

Methylcellulose colony-forming assay

HL-60, U937, THP-1, and MOLM-14 cells were infected with shRNAs directed against a scrambled control (shControl), GSK-3α, or GSK-3β (2 unique constructs per gene) (see Supplemental Table 3 for hairpin sequences). After 48 hours of selection, cells were counted by the trypan blue exclusion assay, and 3×10^4 cells were plated at 1:10 (v/v) in methylcellulose (ClonaCell-TCS Medium) with 1% PS and 1 μg/ml puromycin.

Luciferase assay

Cell lines stably transfected with the β-catenin reporter 7xTCF-luc-puro were counted and lysed in 1X Passive Lysis Buffer (Promega) for 15 minutes. Luciferase Assay Substrate (Promega) was added, and samples were incubated for 2 minutes in the dark. Luminescence was measured and corrected for viability using CellTiter-Glo as described above.

GE-HTS signature development

Gene expression studies. Marker genes for myeloid differentiation were chosen using previously published Affymetrix AML-related data sets (8). We used an initial collection of 42 genes in the bioactive library screen, a refined set of 19 genes in the RNAi primary screen, and a final group of 32 genes in the secondary RNAi screen, the kinase inhibitor screen, and all other follow-up differentiation assays (see Supplemental Tables 4–6 for probe lists). These genes distinguish AML from either neutrophils or monocytes with $P < 0.05$ by *t* test and distinguish undifferentiated versus differentiated HL-60 cells with ATRA, phorbol 12-myristate 13-acetate, or 1,25-dihydroxyvitamin D3 with $P < 0.05$ by *t* test. The GE-HTS assay using LMA and a fluorescent bead-based detection was performed as previously described (9). Two primary methods were used to compare signature gene induction. The summed score combines expression ratios by adding or subtracting them based on the expected direction of regulation from ATRA-treated positive controls. The weighted summed score combines expression ratios by summing them with a weight and sign determined by the signal-to-noise ratio of each expression ratio for the positive control (ATRA-treated) and negative control (DMSO-treated) samples.

GE-HTS screens

We performed 3 GE-HTS differentiation screens: (a) a bioactive small-molecule library screen, (b) a kinase inhibitor-focused small-molecule library screen, and (c) a kinase-focused shRNA library screen. Hits from these 3 screens were selected using approaches previously described (9). Briefly, plates were filtered and scaled, and 5 scoring algorithms were applied: summed score, weighted summed score, naive Bayes, K-nearest neighbor, and support vector machine.

Bioactive small-molecule library screen. 7,500 HL-60 cells per well, in RPMI medium containing 10% FBS, 1% PS, and 0.3 μM vorinostat (as a differentiation enhancer), were plated by MATRIX WellMate in 384-well cell culture plates. 3,517 compounds from the Spectrum/Prestwick Bioactives library and Harvard Stem Cells Bioactives library were screened in triplicate. 10 nl of each compound was pin transferred by CyBi-Well to a final concentration of 20 μM. Each Spectrum/Prestwick Bioactives library plate contained 32 negative controls (0.3 μM vorinostat) and 32 positive controls (0.3 μM vorinostat plus 1 μM ATRA). Plates with compounds from the Harvard Stem Cell Bioactive library contained only negative controls. Plates were incubated at 37°C for 24 hours, followed by measurement of the GE-HTS signature. See Supplemental Table 5 for the probe list.

Kinase inhibitor small-molecule library screen. We independently screened a collection of 84 kinase inhibitors at 8 different doses in triplicate in HL-60 and U937 cells. HL-60 cells were plated at 7,500 cells per well, while U937 cells were plated at 5,000 cells per well. 100 nl compound was then pin transferred by CyBi-Well to appropriate wells. Sixteen 0.2% DMSO-containing negative control wells and eight 1 μM ATRA-containing wells were subsequently pin transferred using a mask plate. Plates were incubated at 37°C for 72 hours, followed by measurement of the GE-HTS differentiation signature. See Supplemental Table 6 for the probe list.

shRNA screen. High-throughput screening was performed with the RNAi Platform at the Broad Institute. As previously reported by Hahn et al., HL-60 cells were plated in 384-well format in 30 μl of medium at 15,000 cells per well and incubated overnight at 37°C with 5% CO_2 (9). Polybrene (Sigma-Aldrich) was added to a final concentration of 8 μg/ml. Approximately 5,000 shRNAs targeting 1,000 genes in a kinome-focused sublibrary of The RNAi Consortium shRNA library were screened in quadruplicate (http://www.broad.mit.edu/rnai/trc/lib) (47). Virus was added at 2.5 μl per well, and plates were spun for 30 minutes at 1,050 *g* and incubated for 48 hours. Selection was performed on 3 replicates with 1 μg/ml puromycin (Sigma-Aldrich), and medium was changed on the unselected control plate. Uninfected controls included untreated cells (8 wells), 1 μM ATRA (8 wells), and 25 μM gefitinib (8 wells). Plates were incubated for 72 hours and then were assessed for differentiation by GE-HTS and viability as described above. An shRNA was considered a hit if it was classified as being more like ATRA-treated controls than untreated HL-60 controls by all 5 scoring algorithms. A secondary screen was performed as described above with the following exceptions: HL-60 and U937 cells were plated at 15,000 cells per well and 4,500 cells per well, respectively. shRNAs against the 132 genes that scored in the primary screen, as well as newly available shRNAs, were screened in 5 replicates. Plates were incubated for 72 hours and then differentiation was assessed by GE-HTS, and viability was measured as described above. See Supplemental Table 4 for the probe list used in the primary screen and Supplemental Table 6 for the probe list used in the secondary screen.

Genome-wide expression analysis

The AML cell lines, MOLM-14, U937, THP-1, and HL-60, were infected with a scrambled control shRNA (shControl), 2 shRNAs directed against GSK-3β (shGSK3B_1 and shGSK3B_2), and 2 shRNAs directed against GSK-3α (shGSK3A_5 and shGSK3A_6). Cells were selected 48 hours after infection with 1 μg/ml puromycin. Forty-eight hours later, protein was extracted as described above. RNA was extracted using the RNeasy Kit and on column digestion of DNA (Qiagen). Knockdown of GSK-3α and GSK-3β was confirmed by Western blot. For each cell line, 3 shControl, 2 shGSK3B_1, 2 shGSK3B_2, 2 shGSK3A_5, and 2 shGSK3A_6 biological replicates were profiled using the Affymetrix HG-U133A HTA (Affymetrix) at the Broad Institute. Gene expression data are available from GEO (accession no. GSE35200; http://www.ncbi.nlm.nih.gov/geo). The RMA algorithm in the Bioconductor package of R was used to process the raw expression data. Two data sets were created: one with all shControl and GSK-3α samples and one with all shControl and GSK-3β samples (12 vs. 16 samples in each case). Each of these data sets was analyzed using GSEA (48) (http://www.broadinstitute.org/gsea/index.jsp), using the curated gene sets from version 2.5 of the Molecular Signatures Database (http://www.broadinstitute.org/gsea/msigdb/index.jsp). Gene sets were scored using the signal-to-noise ratio in the weighted enrichment score, and *P* values were calculated using 1,000 permutations of the phenotype.

The monocyte signature used in GSEA was derived from the hematopoietic gene expression differentiation map (DMAP) database, as described in the Supplemental Information of Novershtern et al. (19). The monocyte versus hematopoietic stem cell upregulated gene set (DMAP_MONO_vs_HSC_UP) was defined as the top 470 genes having significantly higher levels of expression in the DMAP monocyte versus hematopoietic stem cell classes. The monocyte versus hematopoietic stem cell downregulated gene set (DMAP_MONO_vs_HSC_DN) was identified as the top 204 genes having significantly lower levels of expression in the DMAP monocyte versus hematopoietic stem cell classes. The significance of the differential expression was estimated based on the signal-to-noise test for a P value of less than 0.05 and false discovery rate of less than 0.10.

In vivo studies

U937 cells were transduced with the pMMP-LucNeo retrovirus and selected with neomycin at 1 mg/ml. All xenograft studies were performed by injecting luciferase-expressing AML cells via the tail vein into 6- to 8-week-old NSG mice (The Jackson Laboratory). Leukemic disease burden was serially assessed using noninvasive bioluminescence imaging by injecting mice with 75 mg/kg i.p. D-Luciferin (Promega), anesthetizing them with 2%–3% isoflurane, and imaging them on an IVIS Spectrum (Caliper Life Sciences). A standardized region of interest (ROI) encompassing the entire mouse was used to determine total body bioluminescence, with data expressed as photons/s/ROI (ph/s/ROI).

U937-LucNeo cells were transduced with lentiviruses encoding shRNAs targeting GSK-3α (shGSK3A_5, shGSK3A_6, shGSK3A_8, shGSK3A_9), GSK-3β (shGSK3B_1, shGSK3B_2, shGSK3B_4, shGSK3B_7), or LacZ (shControl_2). Transduced cells were selected with 1 μg/ml puromycin for 48 hours, and viable cells were counted using trypan blue exclusion. A standardized number of 1.5×10^6 cells per mouse was injected via tail vein in the xenograft study of shGSK3A_5, shGSK3B_2, and shControl_2, and 2.1×10^6 cells per mouse were injected in the xenograft study comparing shGSK3A_6, shGSK3B_1, and shControl_2 ($n = 6$ in all groups). For the study comparing shGSK3A_8, shGSK3A_9, shGSK3B_4, shGSK3B_7, and shControl_2, mice were injected with 4×10^6 cells per mouse ($n = 6$ in all groups).

All studies were conducted under the auspices of protocols approved by the Dana-Farber Cancer Institute Animal Care and Use Committee.

Statistics

Statistical significance was determined by 2-tailed Student's t test for pair-wise comparison of groups and by log-rank test for survival curves. One-way ANOVA with Tukey's multiple comparison test was used when comparing more than 2 unmatched groups. Two-way repeated-measures ANOVA with Bonferroni correction was used for comparisons of 2 or more groups over a time course.

Acknowledgments

We thank Serena Silver, Jen Grenier, and David Root for RNAi screening guidance and the Chemical Biology Platform at the Broad Institute. We thank all of the patients who contributed invaluable primary samples. We thank Alexandre Puissant, Annie Carlton, and Jacob Berchuck for their technical advice and assistance. This work was supported by the National Cancer Institute (R01 CA140292) (to K. Stegmaier), the American Cancer Society (to K. Stegmaier), an ASH Fellow Scholar Award in Clinical/Translational Research (to K. Stegmaier), Howard Hughes Medical Institute (to K. Stegmaier and L.S. Li), a Smith Family New Investigator Award supported by the Richard Allan Barry Fund at the Boston Foundation (to K. Stegmaier), CancerCare Manitoba (to V. Banerji), CancerCare Manitoba Foundation (to V. Banerji), the University of Manitoba (to V. Banerji), and the Terry Fox Foundation through an award from the National Cancer Institute of Canada (to V. Banerji).

Received for publication January 19, 2011, and accepted in revised form January 4, 2012.

Address correspondence to: Kimberly Stegmaier, Dana-Farber Cancer Institute, 450 Brookline Avenue, Boston, Massachusetts 02215, USA. Phone: 617.632.4438; Fax: 617.632.4850; E-mail: kimberly_stegmaier@dfci.harvard.edu.

Versha Banerji's present address is: Manitoba Institute of Cell Biology and CancerCare Manitoba, Department of Internal Medicine, University of Manitoba, Winnipeg, Manitoba, Canada.

1. Abdel-Wahab O, Levine RL. Recent advances in the treatment of acute myeloid leukemia. *F1000 Med Rep*. 2010;2:55.
2. Rubnitz JE, Gibson B, Smith FO. Acute myeloid leukemia. *Hematol Oncol Clin North Am*. 2010; 24(1):35–63.
3. Dohner H, et al. Diagnosis and management of acute myeloid leukemia in adults: recommendations from an international expert panel, on behalf of the European LeukemiaNet. *Blood*. 2010;115(3):453–474.
4. Ley TJ, et al. DNMT3A mutations in acute myeloid leukemia. *N Engl J Med*. 2010;363(25):2424–2433.
5. Mardis ER, et al. Recurring mutations found by sequencing an acute myeloid leukemia genome. *N Engl J Med*. 2009;361(11):1058–1066.
6. Gilliland DG. Hematologic malignancies. *Curr Opin Hematol*. 2001;8(4):189–191.
7. Ades L, et al. Very long-term outcome of acute promyelocytic leukemia after treatment with all-trans retinoic acid and chemotherapy: the European APL Group experience. *Blood*. 2010;115(9):1690–1696.
8. Stegmaier K, Ross KN, Colavito SA, O'Malley S, Stockwell BR, Golub TR. Gene expression-based high-throughput screening(GE-HTS) and application to leukemia differentiation. *Nat Genet*. 2004;36(3):257–263.
9. Hahn CK, et al. Proteomic and genetic approaches identify Syk as an AML target. *Cancer Cell*. 2009; 16(4):281–294.
10. Peck D, Crawford ED, Ross KN, Stegmaier K, Golub TR, Lamb J. A method for high-throughput gene expression signature analysis. *Genome Biol*. 2006;7(7):R61.
11. Doble BW, Woodgett JR. GSK-3: tricks of the trade for a multi-tasking kinase. *J Cell Sci*. 2003; 116(pt 7):1175–1186.
12. Frame S, Cohen P. GSK3 takes centre stage more than 20 years after its discovery. *Biochem J*. 2001; 359(pt 1):1–16.
13. Wang Z, et al. GSK-3 promotes conditional association of CREB and its coactivators with MEIS1 to facilitate HOX-mediated transcription and oncogenesis. *Cancer Cell*. 2010;17(6):597–608.
14. Abrahamsson AE, et al. Glycogen synthase kinase 3beta missplicing contributes to leukemia stem cell generation. *Proc Natl Acad Sci U S A*. 2009; 106(10):3925–3929.
15. Ougolkov AV, Bone ND, Fernandez-Zapico ME, Kay NE, Billadeau DD. Inhibition of glycogen synthase kinase-3 activity leads to epigenetic silencing of nuclear factor kappaB target genes and induction of apoptosis in chronic lymphocytic leukemia B cells. *Blood*. 2007;110(2):735–742.
16. Song EY, et al. Glycogen synthase kinase--3beta inhibitors suppress leukemia cell growth. *Exp Hematol*. 2010;38(10):908–921.
17. Wang Z, Smith KS, Murphy M, Piloto O, Somervaille TC, Cleary ML. Glycogen synthase kinase 3 in MLL leukaemia maintenance and targeted therapy. *Nature*. 2008;455(7217):1205–1209.
18. Bilim V, et al. Glycogen synthase kinase-3: a new therapeutic target in renal cell carcinoma. *Br J Cancer*. 2009;101(12):2005–2014.
19. Novershtern N, et al. Densely interconnected transcriptional circuits control cell states in human hematopoiesis. *Cell*. 2011;144(2):296–309.
20. Wang Y, et al. The Wnt/beta-catenin pathway is required for the development of leukemia stem cells in AML. *Science*. 2010;327(5973):1650–1653.
21. Yeung J, et al. beta-catenin mediates the establishment and drug resistance of MLL leukemic stem cells. *Cancer Cell*. 2010;18(6):606–618.
22. Doble BW, Patel S, Wood GA, Kockeritz LK, Woodgett JR. Functional redundancy of GSK-3alpha and GSK-3beta in Wnt/beta-catenin signaling shown by using an allelic series of embryonic stem cell lines. *Dev Cell*. 2007;12(6):957–971.
23. Trowbridge JJ, Xenocostas A, Moon RT, Bhatia M. Glycogen synthase kinase-3 is an in vivo regulator of hematopoietic stem cell repopulation. *Nat Med*. 2006;12(1):89–98.
24. Huang J, et al. Pivotal role for glycogen synthase kinase-3 in hematopoietic stem cell homeostasis in mice. *J Clin Invest*. 2009;119(12):3519–3529.
25. Hooper C, Killick R, Lovestone S. The GSK3 hypothesis of Alzheimer's disease. *J Neurochem*. 2008; 104(6):1433–1439.

26. MacAulay K, Woodgett JR. Targeting glycogen synthase kinase-3 (GSK-3) in the treatment of Type 2 diabetes. *Expert Opin Ther Targets*. 2008; 12(10):1265–1274.
27. Gould TD, Zarate CA, Manji HK. Glycogen synthase kinase-3: a target for novel bipolar disorder treatments. *J Clin Psychiatry*. 2004;65(1):10–21.
28. Zhou Y, Uddin S, Zimmerman T, Kang JA, Ulaszek J, Wickrema A. Growth control of multiple myeloma cells through inhibition of glycogen synthase kinase-3. *Leuk Lymphoma*. 2008;49(10):1945–1953.
29. Piazza F, et al. Glycogen Synthase Kinase-3 regulates multiple myeloma cell growth and bortezomib-induced cell death. *BMC Cancer*. 2010;10:526.
30. Zuber J, et al. RNAi screen identifies Brd4 as a therapeutic target in acute myeloid leukaemia. *Nature*. 2011;478(7370):524–528.
31. Archbold HC, Yang YX, Chen L, Cadigan KM. How do they do Wnt they do?: regulation of transcription by the Wnt/beta-catenin pathway. *Acta Physiol (Oxf)*. 2012;204(1):74–109.
32. Cohen P, Frame S. The renaissance of GSK3. *Nat Rev Mol Cell Biol*. 2001;2(10):769–776.
33. Mayfield D, Brown RG. The clinical laboratory and electroencephalographic effects of lithium. *J Psychiatr Res*. 1966;4(3):207–219.
34. Charron D, Barrett AJ, Faille A, Alby N, Schmitt T, Degos L. Lithium in acute myeloid leukaemia. *Lancet*. 1977;1(8025):1307.
35. Visca U, et al. Prevention of antiblastic neutropenia with lithium carbonate. *Lancet*. 1979;1(8119):779.
36. Collado S, Charron D, Degos L. Double-blind, placebo-controlled lithium treatment in chemotherapy induced aplasia for AML: reduced antibiotic requirement. *Med Oncol Tumor Pharmacother*. 1988; 5(2):103–105.
37. Stein RS, Vogler WR, Lefante J. Failure of lithium to limit neutropenia significantly during induction therapy of acute myelogenous leukemia. A Southeastern Cancer Study Group study. *Am J Clin Oncol*. 1984;7(4):365–369.
38. MacAulay K, et al. Glycogen synthase kinase 3alpha-specific regulation of murine hepatic glycogen metabolism. *Cell Metab*. 2007;6(4):329–337.
39. Kaidanovich-Beilin O, et al. Abnormalities in brain structure and behavior in GSK-3alpha mutant mice. *Mol Brain*. 2009;2:35.
40. Hoeflich KP, Luo J, Rubie EA, Tsao MS, Jin O, Woodgett JR. Requirement for glycogen synthase kinase-3beta in cell survival and NF-kappaB activation. *Nature*. 2000;406(6791):86–90.
41. Beg AA, Sha WC, Bronson RT, Ghosh S, Baltimore D. Embryonic lethality and liver degeneration in mice lacking the RelA component of NF-kappa B. *Nature*. 1995;376(6536):167–170.
42. Adachi S, Leoni LM, Carson DA, Nakahata T. Apoptosis induced by molecular targeting therapy in hematological malignancies. *Acta Haematol*. 2004; 111(1–2):107–123.
43. Cho J, Rameshwar P, Sadoshima J. Distinct roles of glycogen synthase kinase (GSK)-3alpha and GSK-3beta in mediating cardiomyocyte differentiation in murine bone marrow-derived mesenchymal stem cells. *J Biol Chem*. 2009;284(52):36647–36658.
44. Lal H, et al. GSK-3alpha limits ischemic injury, cardiac rupture, post- myocardial infarction remodeling and death. *Circulation*. 2012;125(1):65–75.
45. Kong D, Yamori T. Advances in development of phosphatidylinositol 3-kinase inhibitors. *Curr Med Chem*. 2009;16(22):2839–2854.
46. Zhang N, Zhong R, Yan H, Jiang Y. Structural features underlying selective inhibition of GSK3beta by dibromocantharelline: implications for rational drug design. *Chem Biol Drug Des*. 2011;77(3):199–205.
47. Moffat J, et al. A lentiviral RNAi library for human and mouse genes applied to an arrayed viral high-content screen. *Cell*. 2006;124(6):1283–1298.
48. Subramanian A, et al. Gene set enrichment analysis: a knowledge-based approach for interpreting genome-wide expression profiles. *Proc Natl Acad Sci U S A*. 2005;102(43):15545–15550.